JACS
JOURNAL OF THE AMERICAN CHEMICAL SOCIETY

COMMUNICATION

pubs.acs.org/JACS

Sub-10 nm Hexagonal Lanthanide-Doped $NaLuF_4$ Upconversion Nanocrystals for Sensitive Bioimaging in Vivo

Qian Liu, Yun Sun, Tianshe Yang, Wei Feng, Chenguang Li, and Fuyou Li*

Department of Chemistry, Fudan University, Shanghai 200433, P. R. China

Supporting Information

ABSTRACT: By thermal decomposition in the presence only of oleylamine, sub-10 nm hexagonal $NaLuF_4$-based nanocrystals codoped with Gd^{3+}, Yb^{3+}, and Er^{3+} (or Tm^{3+}) have been successfully synthesized. Sub-10 nm β-$NaLuF_4$: 24 mol % Gd^{3+}, 20 mol % Yb^{3+}, 1 mol % Tm^{3+} nanocrystals display bright upconversion luminescence (UCL) with a quantum yield of 0.47 ± 0.06% under continuous-wave excitation at 980 nm. Furthermore, through the use of β-$NaLuF_4$: Gd^{3+},Yb^{3+},Tm^{3+} nanocrystals as a luminescent label, the detection limit of <50 nanocrystal-labeled cells was achieved for whole-body photoluminescent imaging of a small animal (mouse), and high-contrast UCL imaging of a whole-body black mouse with a penetration depth of ∼2 cm was achieved.

Upconversion nanophosphors (UCNPs) have evoked considerable interest for their biological applications because of their unique upconversion luminescence (UCL), namely, the emission of high-energy photons (visible wavelengths) upon excitation by continuous-wave (CW) low-energy photons (near-IR).[1−5] Compared with conventional fluorescent materials, including organic dyes[6] and semiconductor quantum dots,[7] UCNPs can take advantage of CW near-IR (NIR) excitation, thereby eliminating any autofluorescence from biosamples,[3b] minimizing photodamage,[3b] and increasing the penetration depth.[3c,4b] These features make them highly suitable as luminescent labels for bioimaging in vivo.[1g,4]

For application to in vivo imaging in particular, there are some rigorous requirements, such as bright luminescence and small diameter (<10 nm).[6] To date, investigations of sub-10 nm UCNPs have focused on fluoride-based host materials doped with suitable lanthanide ions, because their electronic structures are suitable for the production of strong UCL emission.[8] It is well-known that $NaYF_4$ has been the most efficient host material for upconversion phosphors until now.[9] $NaYF_4$ exists in two phases, the cubic (α) and hexagonal (β) phases [Figure S1 in the Supporting Information (SI)], and the hexagonal phase provides enhanced UCL compared with the cubic phase. For instance, the upconversion efficiency of green emission from hexagonal $NaYF_4$:Yb,Er is ∼10 times that of cubic $NaYF_4$:Yb,Er.[8a,b] The hexagonal form of $NaYF_4$ usually induces larger nanoparticles.[10] Moreover, most of the uniform hexagonal $NaYF_4$ nanoparticles are >10 nm in size,[4c,10a] and reported $NaYF_4$ nanocrystals with sizes of <10 nm have focused on the cubic phase and exhibit relatively weak UCL emission compared with the hexagonal phase.[11] Therefore, it is a great challenge to combine small size (especially sub-10 nm), bright UCL, and hexagonal phase into one nanocrystal. Furthermore, no case of in vivo bioimaging of a small animal using sub-10 nm UCNPs as the luminescent label has been reported to date.[4c] In particular, no detection limit for intramouse UCNP-labeled cells has been reported.

In the present study, by a thermal decomposition reaction in the presence only of oleylamine, we have successfully prepared ∼8 nm hexagonal Gd-doped $NaLuF_4$-based nanocrystals with bright UCL emission. Importantly, the sub-10 nm β-$NaLuF_4$: 24 mol % Gd^{3+}, 20 mol % Yb^{3+}, 1 mol % Tm^{3+} nanocrystals exhibit a high UCL quantum yield of 0.47 ± 0.06% at 800 nm, making them effective as a luminescent probe for monitoring of a whole-body mouse with an excellent detection limit of 50 cells.

$NaLuF_4$ nanocrystals codoped with 20 mol % Yb^{3+}, 2 mol % Er^{3+}, and/or Gd^{3+} were synthesized using a modified thermal decomposition of their corresponding CF_3COO^- salts in oleylamine.[12] X-ray diffraction (XRD) patterns, energy-dispersive X-ray analysis (EDXA) patterns and transmission electron microscopy (TEM) images of the obtained nanocrystals were studied to investigate the effects of the reaction conditions. The physical and chemical properties of the Ln^{3+}-doped $NaLuF_4$ nanocrystals under different conditions are summarized in Table S1 in the SI. It can be seen that the reaction temperature, reaction time, and doping of Gd^{3+} affect the crystal phase and diameter of the $NaLuF_4$ nanocrystals significantly.

At a low temperature (330 °C) using oleylamine as the sole ligand, nanospheres with a size of 18.9 nm were prepared, as determined by TEM (Figure 1a). Their XRD patterns show representative reflections for a cubic phase (Lu1 in Figure 2), indicating that the nanospheres are cubic α-$NaLuF_4$, which was also confirmed by high-resolution TEM (HRTEM) and selected-area electron diffraction (SAED) analysis (Figure 1b). When the reaction temperature was increased to 340 °C without doping with Gd^{3+} ions, nanoparticles with a size of 20.1 nm were formed (Figure 1c). The XRD pattern (Lu2 in Figure 2) can be indexed as a mixture of the cubic and hexagonal phases of $NaLuF_4$. That is, increasing the temperature to 340 °C caused a transition from α to β phase in which the small nanocrystals redissolved and larger ones grew, leading to a broadening of the size distribution.[13]

Although increasing the reaction temperature caused the transition from α-$NaLuF_4$ to β-$NaLuF_4$, the simultaneous enlargement of the size of the $NaLuF_4$ nanocrystals was not as we expected. Recently, Liu and co-workers[10a] reported a Gd^{3+}-doping-induced phase transition of $NaYF_4$ nanocrystals from the α to β phase. Inspired by this result, we introduced Gd^{3+} doping into the synthetic procedure for the $NaLuF_4$ nanocrystals. Doping with 12 mol % Gd^{3+} caused all of the diffraction peaks belonging to the cubic phase to disappear, and the pure hexagonal-phase $NaLuF_4$

Received: July 28, 2011
Published: September 29, 2011

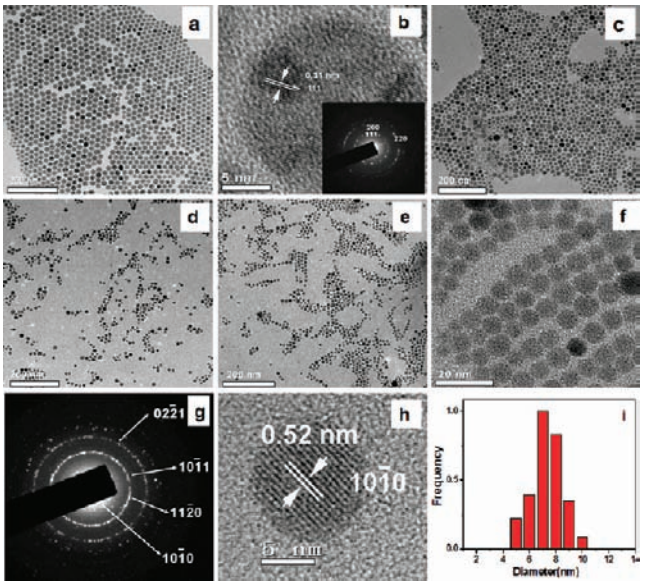

Figure 1. TEM images of (a) Lu1, (c) Lu2, (d) Lu5 and (e, f) Lu6. (b) HRTEM image and (inset) SAED pattern of Lu1. (g, h) SAED pattern and HRTEM image of Lu6. (i) Histogram of the particle size distribution of (e).

nanocrystals were formed (Lu3 in Figure 2), suggesting that the gadolinium helps to mediate the phase transition of $NaLuF_4$ from the cubic to the hexagonal phase. Moreover, the diffraction peaks broadened, indicating a reduction in the average crystallite size. As determined by TEM, the size of the formed spherical nanoparticles decreased to 16.9 nm, in comparison with 20.1 nm for the $NaLuF_4$ nanoparticles without Gd^{3+} doping (Figure S2a,b).

With a further increase of the Gd^{3+} ion concentration to 24 mol %, no extra diffraction peaks were observed (Lu4 in Figure 2), implying the formation of a homogeneous Lu−Gd solid solution, which is consistent with previous observations by Liu and coworkers.[10a] Moreover, reducing the reaction time from 2.5 h (Lu4) to 1 h (Lu5) or 0.25 h (Lu6) with this fixed doping concentration of 24 mol % Gd^{3+} ion afforded only hexagonal-phase $NaLuF_4$ nanocrystals (Figure 2). Meanwhile, the broadening of the diffraction peaks at shorter reaction times implied the formation of smaller nanocrystals. As shown by TEM (Figure 1 and Figures S2 and S3), the diameter of the as-prepared nanocrystals decreased from 12.9 nm for Lu4 to 8.7 nm for Lu5 and 7.8 nm for Lu6. The SAED pattern and HRTEM image of Lu6 (Figure 1g,h) revealed the small nanospheres to be pure hexagonal phase. EDXA revealed the presence of the elements Na, Lu, Yb, F, and Gd in Lu6 (Figure S4). To verify the size distribution of the nanoparticles, dynamic light scattering (DLS) was used. The hydrodynamic diameters of Lu5 and Lu6 in cyclohexane were 9.5 and 8.6 nm, respectively (Figure S5), confirming that sub-10 nm nanocrystals were formed.

The UCL properties of the nanocrystals were then investigated. Herein, for use of UCL emission at 800 nm in bioimaging in vivo, Lu6 nanocrystals doped with 1 mol % Tm^{3+} instead of 2 mol % Er^{3+} (denoted as Lu6-Tm) were prepared. The UCL spectra of Lu6 and Lu6-Tm in cyclohexane under CW excitation from a 980 nm laser (Figure 3a,b) feature the distinct UCL emission bands of Er^{3+} and Tm^{3+}, respectively. For the Lu6 sample, the green emissions at 514−534 and 534−560 nm are the result of transitions from $^2H_{11/2}$ and $^4S_{3/2}$, respectively, to $^4I_{15/2}$ of Er^{3+}. The red emission at 635−680 nm is attributed to the $^4F_{9/2} \rightarrow {}^4I_{15/2}$ transition. For the Lu6-Tm sample, the UCL bands at 475, 695, and

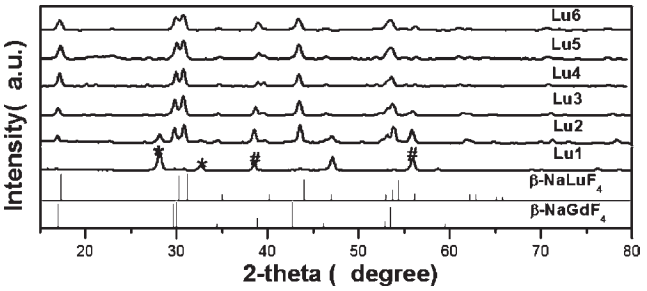

Figure 2. XRD patterns of standard β-$NaGdF_4$, β-$NaLuF_4$, and Lu1−Lu6. Diffraction peaks corresponding to cubic $NaLuF_4$ and NaF are marked with * and #, respectively.

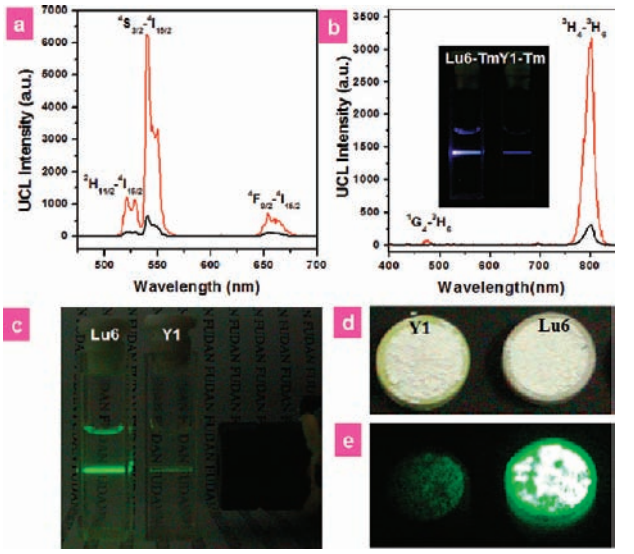

Figure 3. (a, b) UCL spectra of (a) Lu6 (red) and Y1 (black) and (b) Lu6-Tm (red) and Y1-Tm (black) at identical concentrations (3.1 mM) in cyclohexane under CW excitation at 980 nm (power ≈ 200 mW). (c, b inset) UCL emission photos of (c) Lu6 (left) and Y1 (right) and (b inset) Lu6-Tm (left) and Y1-Tm (right) in cyclohexane solution (3.1 mM). (d) Bright-field imaging and (e) UCL emission photos of (left) Y1 and (right) Lu6 powders. A 950 nm short-pass filter was used in (e).

800 nm originate from the $^1G_4 \rightarrow {}^3H_6$, $^3F_3 \rightarrow {}^3H_6$, and $^3H_4 \rightarrow {}^3H_6$ transitions of Tm^{3+}, respectively. Although the band at 475 nm is relatively weak, a blue UCL emission visible to the naked eye was still observed. The energy level diagrams of Gd^{3+}, Yb^{3+}, and Er^{3+}/Tm^{3+} ion as well as that for the UCL mechanism are presented in Figure S6. The UCL spectra of Lu1−Lu5 are similar to that of Lu6 (Figure S7).

Compared with hexagonal-phase $NaYF_4$-based nanocrystals (Y1) with a size of 20 nm (Figure S8), the 7.8 nm Lu6 nanocrystals show a more intense UCL emission at the same concentration of 3.1 mM in cyclohexane (Figure 3c; the CW excitation first illuminated the solution of Y1 and then the solution of Lu6). Although CW 980 nm light excitation was first absorbed by the solution of Y1, Lu6 displays a more intense green UCL emission than Y1 does. Significantly, Lu6 is dominant with green UCL visible to the naked eye. Further investigation by luminescence spectroscopy showed a 9.7-fold enhancement of the UCL intensity at 541 nm for Lu6 relative to Y1 (Figure 3a). Similarly, relative to 20 nm Y1-Tm at the same concentration of 3.1 mM, 7.8 nm Lu6-Tm nanocrystals showed an 11.4-fold-enhanced UCL emission at 800 nm under excitation at the same power

dx.doi.org/10.1021/ja207078s |J. Am. Chem. Soc. 2011, 133, 17122–17125

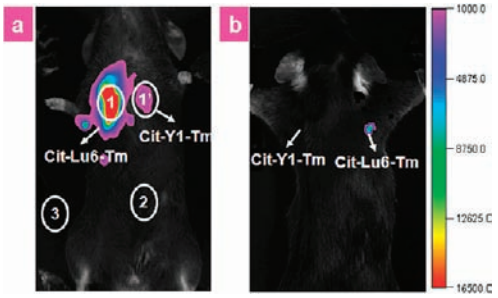

Figure 4. In vivo imaging of a black mouse by subcutaneous injection of cit-Lu6-Tm and cit-Y1-Tm with detection from (a) the chest side and (b) from the back side (λ_{ex} = 980 nm, λ_{em} = 800 ± 10 nm).

density (Figure 3b). This was also confirmed by photographs of their UCL emission (Figure 3b inset).

In addition, we investigated the UCL properties of the nanocrystals in powder form. Two 0.7 cm diameter circles were filled with Lu6 (7.8 nm) and Y1 (20 nm) powders (Figure 3d) and illuminated with CW laser excitation at 980 nm (6 cm beam diameter, 100 mW cm^{-2} power density). The UCL emission was then photographed with a camera (Nikon Coolpix 4500, with a 950 nm short-pass filter). As shown in Figure 3e, bright green UCL emission was captured for Lu6, whereas Y1 displayed significantly weaker emission. Furthermore, the UCL imaging system designed by our group (Figure S9)[4b] was used to perform a quantitative comparison of the UCL emission from the two nanocrystals powders. The UCL emission intensity of Lu6 (7.8 nm) was ~10 times stronger than that of Y1 (Figure S9c). In terms of upconversion materials, the lifetimes showed a positive correlation with the UCL quantum yield (QY). The decay times of Lu6, Y1, Lu6-Tm, and Y1-Tm were also investigated. As shown in Figure S10, the UCL lifetimes of the $^4H_{11/2}$ and $^4F_{9/2}$ levels of Er^{3+} ions in Lu6 are longer than those of Y1. Similarly, the UCL lifetimes of $^3H_4$ and $^1G_4$ of Tm^{3+} in Lu6-Tm are longer than those of Y1-Tm. In particular, the UCL lifetime at 800 nm, which is favorable for in vivo imaging, was measured to be >1 ms.[14] Therefore, the enhanced UCL emission is ascribed to the suppression of nonradiative processes in Lu6.[14] Finally, according to the report by Boyer and van Veggle,[15] the absolute UCL quantum yield of 0.47 ± 0.06% at 800 nm for the $^3H_4 \rightarrow {}^3H_6$ transition of powder Lu6-Tm (7.8 nm) at an excitation power density of 17.5 W cm^{-2}. To the best of our knowledge, this is the first report of small (sub-10 nm) UCNPs producing such a high UCL efficiency.

The monodispersed nanocrystals were then employed as luminescent probes for biological applications. First, the hydrophobic Lu6-Tm and Y1-Tm nanoparticles were converted into hydrophilic ones by replacing the surface oleylamine with citric acid.[16] In this work, the citric acid-coated Lu6-Tm and Y1-Tm are denoted as cit-Lu6-Tm and cit-Y1-Tm, respectively. It can be seen from the TEM image (Figure S11a) that this ligand exchange had no obvious influence on the size and shape of the UCNPs. As determined by DLS, the hydrodynamic diameter of cit-Lu6-Tm in water was 10.8 nm (Figure S5c). Under CW excitation at 980 nm, cit-Lu6-Tm in water displayed intense characteristic UCL emission from Tm^{3+} that peaked at 475 and 800 nm (Figure S11b).

To confirm further the penetration depth of cit-Lu6-Tm for UCL imaging in vivo, a black mouse was selected as a model animal. As far as we know, a black mouse has never been used to investigate the penetration depth of conventional fluorescent materials because of the strong absorption of excitation and emission. As shown in

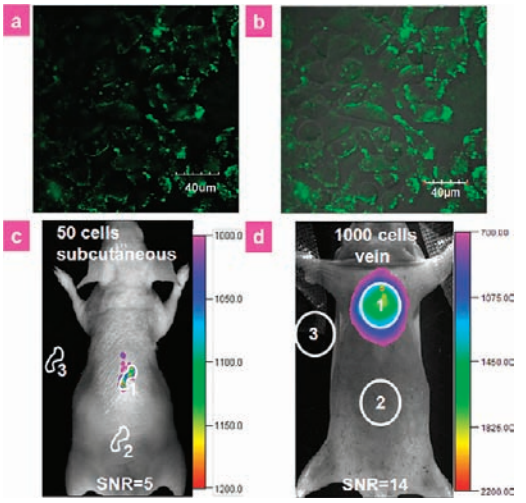

Figure 5. (a) Confocal UCL image and (b) its overlay with a bright-field image of cells stained with 200 μg mL^{-1} cit-Lu6-Tm for 2 h at 37 °C (λ_{ex}= 980 nm, λ_{em}= 450−490 nm). (c, d) In vivo UCL imaging of athymic nude mice after (a) subcutaneous injection of 50 KB cells and (d) vein injection of 1000 cells. The KB cells were incubated with 200 μg mL^{-1} cit-Lu6-Tm for 2 h. SNR = [(mean luminescence intensity of 1) − (mean luminescence intensity of 3)]/[(mean luminescence intensity of 2) − (mean luminescence intensity of 3)].

Figure 4a and Table S2, the signal-to-noise ratio (SNR) of a black mouse injected subcutaneously with cit-Lu6-Tm is 12-fold larger than that with cit-Y1-Tm. The UCL signal from cit-Lu6-Tm also can be detected even from the back side (Figure 4b), suggesting that high-contrast UCL imaging of a whole-body black mouse with a penetration depth of ~2 cm was achieved. This shows that Lu6 has great penetration capability.

Furthermore, the interaction of cit-Lu6-Tm with living cells was investigated. The effect of cit-Lu6-Tm on cell proliferation of KB cells was determined using an in vitro toxicology assay kit (Figure S12). The viability of untreated cells was assumed to be 100%. Upon incubation with cit-Lu6-Tm (100 μg mL^{-1}) for 5 and 24 h, fewer than 10% of the KB cells died. When the concentration of cit-Lu6-Tm was increased to 800 μg mL^{-1}, the cell viability still remained above 80%. These results show that the cit-Lu6-Tm has low toxicity toward cell proliferation.

A laser-scanning UCL microscope (LSUCLM)[3b] was used to investigate the luminescent imaging of living cells. After incubation with 200 μg mL^{-1} cit-Lu6-Tm in phosphate-buffered saline (pH 7) for 2 h at 37 °C, the unbound nanocrystals were washed away, and the living cells were imaged using 980 nm excitation (Figure 5a). Intense intracellular UCL emission was observed with a high signal-to-background ratio (background counts of ~0) (Figure S13). Overlays of confocal luminescence imaging and bright-field images (Figure 5b) demonstrated that the luminescence was evident in the intracellular region, which was confirmed by Z-scan confocal UCL imaging (Figure S14). This result indicated that the cit-Lu6-Tm could be used as a luminescence probe for cell imaging.

In the previous literature, it is often mentioned that UCL-based probes show high penetration depth and low autofluorescence from biosamples. Liu and co-workers[4i] reported that the penetration depth in tissue reached 0.8 cm using 30 nm β-$NaYF_4$:Yb,Er UCNPs as luminescent probes. Until now, no data concerning the penetration depth and sensitivity of UCL bioimaging in vivo have been reported. The detection limit of UCNP-labeled cells is very important for evaluation of the sensitivity of bioimaging in vivo.

By subcutaneous injection of cit-Lu6-Tm-labeled KB cells into a nude mouse, the detection threshold of cit-Lu6-Tm-labeled cells was measured. As shown in Figure 5c, a UCL signal can be detected with SNR > 3 for a nude mouse injected subcutaneously with 50 cit-Lu6-Tm-labeled KB cells under 980 nm excitation at 120 mW cm^{-2}, indicating that the detection limit of UCNP-labeled cells injected subcutaneously is <50.

In addition, the intramouse detection limit for UCNP-labeled cells was also examined. As shown in Figure 5d, after intravenous injection of 1000 cit-Lu6-Tm-labeled KB cells into a 30 g naked mouse, high-contrast in vivo UCL imaging of the whole-body mouse was achieved with SNR > 10, meaning that the intramouse detection limit of UCNP-labeled cells is <1000. To the best of our knowledge, this is the first report describing an intramouse detection limit of <1000 nanocrystal-labeled cells for whole-body UCL imaging of a small animal.

To summarize, sub-10 nm Gd^{3+}-doped β-$NaLuF_4$ nanocrystals material with bright upconversion luminescence have been synthesized by thermal decomposition in the presence of oleylamine. Such sub-10 nm β-$NaLuF_4$:Gd,Yb,Tm nanocrystals display bright UCL emission with a quantum yield of 0.47 ± 0.06%, indicating that sub-10 nm hexagonal $NaLuF_4$:Gd^{3+},Yb^{3+},Tm^{3+} (7.8 nm) is an excellent nanomaterial for upconversion emission. With such sub-10 nm β-$NaLuF_4$:Gd,Yb,Tm nanocrystals as a UCL probe, excellent detection limits of 50 and 1000 nanocrystal-labeled cells were achieved for subcutaneous and intravenous injection, respectively. In particular, high-contrast UCL imaging of a whole-body black mouse with a penetration depth of ∼2 cm was achieved. The use of $NaLuF_4$ as a host material provides a new strategy for the fabrication of bright upconversion nanocrystals for further applications in biological science and medicine.

■ ASSOCIATED CONTENT

Supporting Information. Synthesis, experimental details, and additional data. This material is available free of charge via the Internet at http://pubs.acs.org.

■ AUTHOR INFORMATION

Corresponding Author
fyli@fudan.edu.cn

■ ACKNOWLEDGMENT

The authors thank the NSFC (20825101 and 91027004), the State Key Basic Research Program of China (2011AA03A407 and 2012CB932403), Shanghai Sci. Tech. Comm. (11XD1400200 and 1052nm03400), IRT0911, and B108 for financial support. We also thank Prof. X. Y. Chen for help with the UCL lifetime measurement.

■ REFERENCES

(1) (a) Auzel, F. *Chem. Rev.* **2004**, *104*, 139. (b) Wang, F.; Liu, X. G. *Chem. Soc. Rev.* **2009**, *38*, 976. (c) Li, C.; Lin, J. *J. Mater. Chem.* **2010**, *20*, 6831. (d) Feng, W.; Sun, L. D.; Zhang, Y. W.; Yan, C. H. *Coord. Chem. Rev.* **2010**, *254*, 1038. (e) Wang, F.; Banerjee, D.; Liu, Y. S.; Chen, X. Y.; Liu, X. G. *Analyst* **2010**, *135*, 1839. (f) Haase, M.; Schäfer, H. *Angew. Chem., Int. Ed.* **2011**, *50*, 5808.(g) Zhou, J.; Liu, Z.; Li, F. Y. *Chem. Soc. Rev.* **2011**, DOI: 10.1039/C1CS15187H.

(2) Chen, Z. G.; Chen, H. L.; Hu, H.; Yu, M. X.; Li, F. Y.; Zhang, Q.; Zhou, Z. G.; Yi, T.; Huang, C. H. *J. Am. Chem. Soc.* **2008**, *130*, 3023.

(3) (a) Hu, H.; Yu, M. X.; Li, F. Y.; Chen, Z. G.; Gao, X.; Xiong, L. Q.; Huang, C. H. *Chem. Mater.* **2008**, *20*, 7003. (b) Yu, M. X.; Li, F. Y.; Chen, Z. G.; Hu, H.; Zhan, C.; Huang, C. H. *Anal. Chem.* **2009**, *81*, 930. (c) Idris, N. M.; Li, Z. Q.; Ye, L.; Sim, E. K. W.; Mahendran, R.; Ho, P. C. L.; Zhang, Y. *Biomaterials* **2009**, *30*, 5104. (d) Chatterjee, D. K.; Rufaihah, A. J.; Zhang, Y. *Biomaterials* **2008**, *29*, 937. (e) Zhang, F.; Braun, G. B.; Shi, Y. F.; Zhang, Y. C.; Sun, X. H.; Reich, N. O.; Zhao, D. Y.; Stucky, G. *J. Am. Chem. Soc.* **2010**, *132*, 2850. (f) Wu, S. W.; Han, G.; Milliron, D. J.; Aloni, S.; Altoe, V.; Talapin, D. V.; Cohen, B. E.; Schuck, P. J. *Proc. Natl. Acad. Sci. U.S.A.* **2009**, *106*, 10917. (g) Wang, M.; Mi, C. C.; Wang, W. X.; Liu, C. H.; Wu, Y. F.; Xu, Z. R.; Mao, C. B.; Xu, S. K. *ACS Nano* **2009**, *3*, 1580.(h) Liu, Q.; Peng, J. J.; Sun, L. N.; Li, F. Y. *ACS Nano* [Online early access]. DOI: 10.1021/nn202620u. Published Online: Sept 7, 2011. (i) Liu, J. L.; Liu, Y.; Liu, Q.; Li, C. Y.; Sun, L. N.; Li, F. Y. *J. Am. Chem. Soc.* **2011**, *133*, 15276.

(4) (a) Nyk, M.; Kumar, R.; Ohulchanskyy, T. Y.; Bergey, E. J.; Prasad, P. N. *Nano Lett.* **2008**, *8*, 3834. (b) Xiong, L. Q.; Chen, Z. G.; Tian, Q. W.; Cao, T. Y.; Xu, C. J.; Li, F. Y. *Anal. Chem.* **2009**, *81*, 8687. (c) Xiong, L. Q.; Yang, T. S.; Yang, Y.; Xu, C. J.; Li, F. Y. *Biomaterials* **2010**, *31*, 7078. (d) Zhou, J.; Sun, Y.; Du, X. X.; Xiong, L. Q.; Hu, H.; Li, F. Y. *Biomaterials* **2010**, *31*, 3287. (e) Zhou, J.; Yu, M. X.; Sun, Y.; Zhang, X. Z.; Zhu, X. J.; Wu, Z. H.; Wu, D. M.; Li, F. Y. *Biomaterials* **2011**, *32*, 1148. (f) Liu, Q.; Sun, Y.; Li, C. G.; Zhou, J.; Li, C. Y.; Yang, T. S.; Zhang, X. Z.; Yi, T.; Wu, D. M.; Li, F. Y. *ACS Nano* **2011**, *5*, 3146. (g) Kobayashi, H.; Kosaka, N.; Ogawa, M.; Morgan, N. Y.; Smith, P. D.; Murray, C. B.; Ye, X. C.; Collins, J.; Kumar, G. A.; Bell, H.; Choyke, P. L. *J. Mater. Chem.* **2009**, *19*, 6481. (h) Wang, C.; Chen, L.; Liu, Z. *Biomaterials* **2011**, *32*, 1110. (i) Wang, C.; Tao, H. Q.; Chen, L.; Liu, Z. *Biomaterials* **2011**, *32*, 6145. (j) Wang, Z. L.; Hao, J. H.; Chan, H. L. W.; Law, G. L.; Wong, W. T.; Wong, K. L.; Murphy, M. B.; Su, T.; Zhang, Z. H.; Zeng, S. Q. *Nanoscale* **2011**, *3*, 2175. (k) Cheng, L.; Yang, K.; Li, Y. G.; Chen, J. H.; Wang, C.; Shao, M. W.; Lee, S. T.; Liu, Z. *Angew. Chem., Int. Ed.* **2011**, *50*, 7385. (l) Jiang, S.; Zhang, Y. *Langmuir* **2010**, *26*, 6689.

(5) (a) Gai, S.; Yang, P.; Li, C.; Wang, We.; Dai, Y.; Niu, N.; Lin, J. *Adv. Funct. Mater.* **2010**, *20*, 1166. (b) Fischer, L. H.; Harms, G. S.; Wolfbeis, O. S. *Angew. Chem., Int. Ed.* **2011**, *50*, 4546. (c) Achatz, D. E.; Meier, R. J.; Fischer, L. H.; Wolfbeis, O. S. *Angew. Chem., Int. Ed.* **2011**, *50*, 260.

(6) Kobayashi, H.; Ogawa, M.; Alford, R.; Choyke, P. L.; Urano, Y. *Chem. Rev.* **2010**, *110*, 2620.

(7) (a) Resch-Genger, U.; Grabolle, M.; Cavaliere-Jaricot, S.; Nitschke, R.; Nann, T. *Nat. Methods* **2008**, *5*, 763. (b) Wang, Q. B.; Liu, Y.; Ke, Y. G.; Yan, H. *Angew. Chem., Int. Ed.* **2008**, *47*, 316. (c) Du, Y. P.; Xu, B.; Fu, T.; Cai, M.; Li, F.; Zhang, Y.; Wang, Q. B. *J. Am. Chem. Soc.* **2010**, *132*, 1470. (d) Yu, M. X.; Zhou, C.; Li, J. B.; Hankins, J. D.; Zheng, J. *J. Am. Chem. Soc.* **2011**, *133*, 11014.

(8) (a) Wang, G. F.; Peng, Q.; Li, Y. D. *J. Am. Chem. Soc.* **2009**, *131*, 14200. (b) Krämer, K.; Biner, D.; Frei, G.; Güdel, H.; Hehlen, M.; Lüthi, S. *Chem. Mater.* **2004**, *16*, 1244. (c) Chen, D. Q.; Yu, Y. L.; Huang, F.; Huang, A. P.; Wang, Y. S. *J. Am. Chem. Soc.* **2010**, *132*, 9976. (d) Boyer, J. C.; Cuccia, L. A.; Capobianco, J. A. *Nano Lett.* **2007**, *7*, 847. (e) Du, Y. P.; Sun, X.; Zhang, Y. W.; Yan, Z. G.; Sun, L. D.; Yan, C. H. *Cryst. Growth Des.* **2009**, *9*, 2013.

(9) (a) Mai, H. X.; Zhang, Y. W.; Sun, L. D.; Yan, C. H. *J. Phys. Chem. C* **2007**, *111*, 13730. (b) Boyer, J. C.; Manseau, M. P.; Murray, J. I.; van Veggel, F. C. J. M. *Langmuir* **2010**, *26*, 1157.

(10) (a) Wang, F.; Han, Y.; Lim, C. S.; Lu, Y. H.; Wang, J.; Xu, J.; Chen, H. Y.; Zhang, C.; Hong, M. H.; Liu, X. G. *Nature* **2010**, *463*, 1061. (b) Heer, S.; Kömpe, K.; Güdel, H.; Haase, M. *Adv. Mater.* **2004**, *16*, 2102. (c) Li, C.; Yang, J.; Yang, P.; Zhang, X.; Lian, H.; Lin, J. *Cryst. Growth Des.* **2008**, *8*, 923.

(11) Chen, G. Y.; Ohulchanskyy, T. Y.; Kumar, R.; Agren, H.; Prasad, P. N. *ACS Nano* **2010**, *4*, 3163.

(12) (a) Mai, H. X.; Zhang, Y. W.; Si, R.; Yan, Z. G.; Sun, L. D.; You, L. P.; Yan, C. H. *J. Am. Chem. Soc.* **2006**, *128*, 6426. (b) Boyer, J. C.; Vetrone, F.; Cuccia, L. A.; Capobianco, J. A. *J. Am. Chem. Soc.* **2006**, *128*, 7444.

(13) Yi, G. S.; Chow, G. M. *Adv. Funct. Mater.* **2006**, *16*, 2324.

(14) (a) Liu, Y. S.; Tu, D. T.; Zhu, H. M.; Li, R. F.; Luo, W. Q.; Chen, X. Y. *Adv. Mater.* **2010**, *22*, 3266. (b) Shi, F.; Wang, J. G.; Zhai, X. S.; Zhao, D.; Qin, W. P. *CrystEngComm* **2011**, *13*, 3782.

(15) Boyer, J. C.; van Veggel, F. C. J. M. *Nanoscale* **2010**, *2*, 1417.

(16) Cao, T. Y.; Yang, T. S.; Gao, Y.; Yang, Y.; Hu, H.; Li, F. Y. *Inorg. Chem. Commun.* **2010**, *13*, 392.